Available online at www.sciencedirect.com
ScienceDirect
Journal of Solid State Chemistry 180 (2007) 866–872
JOURNAL OF SOLID STATE CHEMISTRY
www.elsevier.com/locate/jssc

Three-dimensional framework of uranium-centered polyhedra with non-intersecting channels in the uranyl oxy-vanadates $A_2(UO_2)_3(VO_4)_2O$ (A = Li, Na)

S. Obbade*, L. Duvieubourg, C. Dion, F. Abraham

Unité de Catalyse et de Chimie du Solide, UCCS UMR CNRS 8181, ENSCL-USTL, B.P. 90108, 59652 Villeneuve d'Ascq Cedex, France

Received 10 October 2006; received in revised form 6 December 2006; accepted 8 December 2006
Available online 27 December 2006

Abstract

The uranyl vanadates $A_2(UO_2)_3(VO_4)_2O$ (A = Li, Na) have been synthesized by solid-state reaction and the structure of the Li compound was solved from single-crystal X-ray diffraction. The crystal structure is built from $^1_\infty[UO_5]^{4-}$ chains of edge-shared $U(2)O_7$ pentagonal bipyramids alternatively parallel to $\vec{a}$- and $\vec{b}$-axis and further connected together to form a three-dimensional (3-D) arrangement. The perpendicular chains are hung on both sides of a sheet $^2_\infty[(UO_2)(VO_4)_2]^{4-}$ parallel to (001), formed by $U(1)O_6$ square bipyramids connected by VO_4 tetrahedra, and derived from the autunite-type sheet. The resulting 3-D framework creates non-intersecting channels running down the $\vec{a}$- and $\vec{b}$-axis formed by empty face-shared oxygen octahedra, the Li^+ ions are displaced from the center of the channels and occupy the middle of one edge of the common face. The peculiar position of the Li^+ ion together with the full occupancy explain the low conductivity of $Li_2(UO_2)_3(VO_4)_2O$ compared with that of $Na(UO_2)_4(VO_4)_3$ containing the same type of channels half occupied by Na^+ ions in the octahedral sites.

Crystallographic data for $Li_2(UO_2)_3(VO_4)_2O$: tetragonal, space group $I41/amd$, $a = 7.3303(5)$ Å, $c = 24.653(3)$ Å, $V = 1324.7(2)$ Å^3, $Z = 4$, $\rho_{mes} = 5.32(2)$ g/cm^3, $\rho_{cal} = 5.36(3)$ g/cm^3, full-matrix least-squares refinement basis on F^2 yielded, $R_1 = 0.032$, w$R_2 = 0.085$ for 37 refined parameters with 364 independent reflections with $I \geqslant 2\sigma(I)$.
© 2006 Elsevier Inc. All rights reserved.

Keywords: Uranyl vanadate; Crystal structure determination; Solid-state synthesis; Non-intersecting mono-dimensional channels; Cationic conductivity

1. Introduction

The solid-state chemistry of uranyl-containing inorganic compounds has been the focus of considerable attention these last two decades due to their important environment aspect, the possibility of their formation during the storage of spent nuclear fuel and the potentiality of their application in the nuclear industry. Moreover, the structural chemistry of uranyl compounds formed with inorganic oxo-anions is very rich in diversity because of the various coordination polyhedra around U^{6+} (square, pentagonal and hexagonal bipyramids) but also of the various oxoanion geometries (tetrahedron, square pyramid, trigonal pyramid, octahedron) around the transition metals in their highest possible oxidation states (V, Nb, Mo, W …). We have recently reported the preparation and structures of a large number of compounds in the alkali metal–uranyl-vanadate systems [1–8], which magnificently illustrate the variety of coordination geometries and the flexibility of the linkage between polyhedra. When V^{5+} occurs in square pyramids, the vanadyl $V{=}O$ bonds are parallel to the uranyl ions and preclude the association of polyhedra in the direction of these linear elements leading to two-dimensional (2-D) arrangements as in the carnotite-type compounds [1,2,9,10] and in CsUV3O11 [7], the alkaline metals occupying the interspace between the anionic layers. When V^{5+} is in tetrahedral coordination, there is still a tendency to layered structures such as in $A_6[(UO_2)_5(VO_4)_2]O_5]$ with A = Na, K, Rb [4,5], in $A_7[(UO_2)_8(VO_4)_2]O_8Cl]$ with A = Rb, Cs [3], and in $Cs_4U_2V_2O_{13}$ [6]. However, using the smallest A^+ ions

*Corresponding author. Fax: +33 3 20 43 68 14.
E-mail address: said.obbade@ensc-lille.fr (S. Obbade).

0022-4596/$ - see front matter © 2006 Elsevier Inc. All rights reserved.
doi:10.1016/j.jssc.2006.12.014

(Li^+ and Na^+) a three-dimensional (3-D) arrangement has been obtained in the $A(UO_2)_4(VO_4)_3$ compounds [8], exemplifying the key role of the counter ions on the obtained uranyl-vanadate architecture.

In many uranyl oxo-compounds, UO_7 pentagonal bipyramids share opposite equatorial edges to form zig-zag infinite chains $^1_\infty[UO_5]^{4-}$ further connected by sharing the fifth equatorial oxygen atom directly or through oxoanion polyhedra to built layers. In $A(UO_2)_4(VO_4)_3$ ($M = Li$, Na) (8) the $^1_\infty[UO_5]^{4-}$ chains connect together through original new layers $[(UO_2)_2(VO_4)_3]^{5-}$ constituted of VO_4 tetrahedra and UO_6 square bipyramids, creating an open-framework with non-crossing channels. The dimensionality of the polyhedral arrangement largely influences such properties of the compounds as ionic conductivity and in the last compounds large values of conductivity represent the high mobility of the alkaline metals within non-intersecting channels created by the open uranyl-vanadate framework. For this reason, it is interesting to deepen the electrical studies about these channel compounds families.

In this paper, we report the synthesis, the crystal structure and the conductivity properties of a new family of alkali uranyl vanadates $A_2(UO_2)_3(VO_4)_2O$ ($M = Li$, Na), characterized by a novel framework with a 2-D system of perpendicular non-crossing channels and we underline the relationship between the $A_2(UO_2)_3(VO_4)_2O$ and $A(UO_2)_4(VO_4)_3$ series.

2. Experimental

2.1. Synthesis

$A_2(UO_2)_3(VO_4)_2O$ ($A = Li$, Na) powdered samples were synthesized by solid-state reaction between V_2O_5 (Aldrich), U_3O_8 (Prolabo) and A_2CO_3 (Aldrich) mixed in the molar ratio 1:1:1 according to the reaction:

$$A_2CO_3 + U_3O_8 + V_2O_5 + \tfrac{1}{2}O_2 \rightarrow A_2U_3V_2O_{15} + CO_2.$$

The homogeneous mixtures were slowly heated up to 850 °C in a platinum crucible and maintained at this temperature during 1 week, with intermediate coolings and grindings and finally slowly (10 °C/h) cooled to room temperature. After such treatment, for $A = Li$, a new compound is formed with a distinctive X-ray diffraction pattern. For $A = Na$, the corresponding new compound is always accompanied by a very small quantity of impurity identified as $Na(UO_2)_4(VO_4)_3$ phase. The as-prepared powders were melted at 1000 °C and cooled at 2 °C/h to 850 °C and finally at 10 °C/h down to room-temperature. Washing of the obtained yellowish shiny crystalline products with ethanol allowed the separation of yellow single crystals of the new compound $Li_2(UO_2)_3(VO_4)_2O$ for $A = Li$ and of $Na(UO_2)_4(VO_4)_3$ for $A = Na$ [8]. Unfortunately, the change of the experimental conditions (cooling rate and starting sodium salt) did not allow the growth of $Na_2(UO_2)_3(VO_4)_2O$ crystals.

For $Li_2(UO_2)_3(VO_4)_2O$, the X-ray powder diffraction pattern of the powder is identical to that of crushed single crystals and to that of the calculated pattern from the crystal structure results. The unit cell parameters were refined by a least-squares procedure from the indexed powder diffraction pattern, recorded at room temperature, with a Bruker D8 $\theta/2\theta$ diffractometer equipped with a secondary monochromator and corrected for $K\alpha 2$ contribution in Bragg–Brentano geometry, using Cu$K\alpha$ radiation (1.54056 Å), in steps of 0.02° and a counting time of 15 s per step, within an angular range of 5–110° in 2θ . For both compounds, the refined unit cell parameters and the indexed powder patterns with its merit factors $F20$ defined by Smith and Snyder [11] are given in Table 1.

The density measured with an automated Micromeritics Accupy 1330 helium pycnometer using a 1-cm^3 cell, indicates a good agreement between the calculated and measured densities for $Li_2(UO_2)_3(VO_4)_2O$, with four formula per unit cell ($\rho_{mes} = 5.32(2)\ g/cm^3$, $\rho_{cal} = 5.36(3)\ g/cm^3$).

2.2. Single-crystal X-ray diffraction and structure determination

A well-shaped yellow crystal of $Li_2(UO_2)_3(VO_4)_2O$ was selected for X-ray diffraction investigations. The measurement of X-ray intensities was performed at room temperature using a BRUKER AXS diffractometer equipped with a 1K SMART CCD detector and monochromated Mo$K\alpha$ radiation. Details of the data collection are given in Table 2. Before the crystal determination, intensity data were corrected for Lorentz polarization and background effects using the Bruker program SAINT [12]. Then, the absorption corrections based on the precise crystal morphology and indexed crystal faces were applied using the program XPREP of the SHELXTL package [13], followed by SADABS program [14]. The crystal structure of $Li_2(UO_2)_3(VO_4)_2O$ was solved in the $I41/amd$ centrosymmetric space group by means of direct methods strategy using SHELXS program [15] that localize the heavy atoms U and V. The positions of the oxygen and Li atoms were deduced from subsequent refinements and difference Fourier syntheses. The atomic scattering factors for neutral atoms were taken from the "International Tables for X-ray Crystallography" [16]. Refinement of atomic positional parameters, anisotropic displacement parameters for U, V and O atoms, and isotropic displacement parameters for Li yielded the final $R = 0.032$ and $R_w = 0.085$. The atomic positions and the equivalent isotropic displacement factors are given in Table 3. Anisotropic factors for non-Li atoms are given in Table 4.

2.3. Electrical conductivity measurements and thermal analyses

Electrical conductivity measurements were carried out on cylindrical pellets (diameter, 5 mm; thickness, ca. 3 mm)

Table 1
X-Ray powder patterns of $A_2(UO_2)_3(VO_4)_2O$ (A = Li, Na), with X-ray radiation $\lambda(CuK\alpha) = 1.54056$ Å

$Li_2(UO_2)_3(VO_4)_2O$			$Na_2(UO_2)_3(VO_4)_2O$		
hkl	2θ	I_{Obs} (%)	hkl	2θ	I_{Obs} (%)
1 0 1	12.60	15	1 0 1	12.65	17
0 0 4	14.37	3	0 0 4	14.12	1
1 0 3	16.20	20	1 0 3	16.13	37
1 1 2	18.57	41	1 1 2	18.62	97
1 0 5	21.73	57	1 0 5	21.50	76
2 0 0	24.28	100	2 0 0	24.43	100
2 1 1	27.45	6	1 1 6	27.47	12
1 1 6	27.71	15	2 1 1	27.60	10
1 0 7	28.11	47	1 0 7	27.73	60
2 1 3	29.33	17	0 0 8	28.46	4
2 1 5	32.81	20	2 1 3	29.42	18
2 2 0	34.61	36	2 1 5	32.77	21
2 1 7	37.48	35	2 2 0	34.83	27
3 0 3	38.43	4	3 0 1	37.19	2
3 1 2	39.56	41	2 1 7	37.29	22
1 1 10	40.53	28	3 0 3	38.60	5
3 0 5	41.23	23	3 1 2	39.78	41
1 0 11	42.17	3	3 0 5	41.30	14
0 0 12	44.09	18	3 1 4	41.76	2
3 1 6	44.90	17	0 0 12	43.27	10
3 0 7	45.17	26	3 1 6	44.92	10
3 2 3	45.99	4	3 0 7	45.09	16
3 2 5	48.43	21	3 2 3	46.22	4
4 0 0	49.75	34	3 2 5	48.57	20
2 0 12	50.97	34	4 0 0	50.08	38
3 2 7	51.93	32	2 0 12	50.32	34
4 1 3	52.67	2	4 1 1	51.87	12
3 3 2	53.56	15	4 1 3	52.96	3
3 1 10	54.33	35	3 3 2	53.89	14
4 1 5	54.90	16	3 1 10	54.04	27
1 1 14	55.09	5	4 1 5	55.10	18
4 2 0	56.11	33	3 2 9	56.22	2
2 2 12	57.23	17	1 0 15	56.44	14
1 0 15	57.48	2	4 2 0	56.48	32
3 3 6	57.90	2	2 2 12	56.70	14
2 0 14	58.13	24	3 3 6	58.06	4
2 1 15	63.57	2	2 1 15	62.41	4
4 3 3	64.57	1	1 0 17	64.41	7
5 1 2	65.35	4	5 1 2	65.78	3
1 0 17	65.64	14	3 3 10	65.91	15
3 3 10	66.03	14	4 3 5	66.86	4
4 3 5	66.54	14	5 0 5	66.86	4
5 0 5	66.54	4	3 0 15	68.06	7
3 1 14	66.71	17	5 1 6	69.52	11
4 0 12	68.63	16	4 3 7	69.59	1
5 1 6	69.24	2	5 0 7	69.59	1
4 3 7	69.44	4	1 1 18	69.91	8
5 0 7	69.44	8	5 2 3	70.51	1
5 2 3	70.07	2	5 2 5	72.34	6

$Li_2(UO_2)_3(VO_4)_2O$: $a = 7.3245(1)$ Å, $c = 24.627(3)$ Å; F20 = 154 (0.0040; 33).
$Na_2(UO_2)_3(VO_4)_2O$: $a = 7.2793(2)$ Å, $c = 25.067(4)$ Å; F20 = 273 (0.0024; 30).

obtained using a conventional cold press and sintered at 750 °C for 2 days, followed by slow cooling, 5 °C h^{-1}, until room temperature. Gold electrodes were vacuum-deposited on both flat surfaces of the pellets. Conductivity measurements were performed by AC impedance spectroscopy over the range 1–10^6 Hz with a Solartron 1170 frequency-response analyzer. Measurements were made at 20 °C intervals over the range 50–720 °C on both heating and cooling. Each set of values was recorded at a given temperature after a 1 h stabilization time. To determine the thermal stability domain of each compound, differential thermal analyses (DTA) were performed in air with a SETARAM 92-1600 thermal analyzer in the temperature

Table 2
Crystal data, intensity collection and structure refinement parameters $Li_2(UO_2)_3(VO_4)_2O$

Crystal data	
Crystal symmetry	Tetragonal
Space group	$I\,41/amd$
Unit cell parameters (Å)	$a = 7.3303(5)$
(From single crystal)	$c = 24.653(3)$
Cell volume (Å^3)	$V = 1324.7(2)$
Z	4
Calculated density (g/cm^3)	$\rho_{cal} = 5.36(3)$
Measured density (g/cm^3)	$\rho_{mes} = 5.32(2)$
Color	Yellow
Data collection	
Temperature (K)	293(2)
Radiation Mo($K\alpha$)	0.71073 Å
Scan mode	ω
Recording angular range (deg.)	3.72/29.51
Recording reciprocal space	$-10 \leqslant h \leqslant 10$
	$-10 \leqslant h \leqslant 10$
	$-32 \leqslant h \leqslant 32$
Number of reflections	
Measured/independent	3584/364
Absorption μ (cm^{-1})	379.85
Refinement	
Refined parameters/restraints	37/0
Goodness of fit on F^2	0.772
R_1 $[I > 2\sigma(I)]$	0.032
wR_2 $[I > 2\sigma(I)]$	0.085
Largest diff. peak and hole (e Å^{-3})	1.006/−2.503

Note: $R_1 = \Sigma(|F_o|-|F_c|)/\Sigma|F_o|$; $wR_2 = [\Sigma_w(F_o^2—F_c^2)2/\Sigma_w(F_o^2)^2]1/2$; $w = 1/[\sigma^2(F_o^2) + (aP)^2 + bP]$ where a and b are refinable parameters and $P = (F_o^2 + 2F_c^2)/3$.

Table 3
Atomic coordinates with equivalent (U_{eq}) or isotopic (U_{iso}) displacement parameters (Å^2) for $Li_2(UO_2)_3(VO_4)_2O$

Atom	Site	Occup.	x	y	z	U_{eq}/U_{iso}*
U1	4*b*	1	1/2	1/4	1/8	0.0103(3)
U2	8*e*	1	0	1/4	−0.03961(3)	0.0102(3)
V	8*e*	1	0	1/4	0.0933(1)	0.0100(6)
O1	4*a*	1	0	1/4	−1/8	0.013(4)
O2	16*h*	1	0.1898(15)	1/4	0.1338(4)	0.020(2)
O3	8e	1	1/2	1/4	0.0521(6)	0.018(4)
O4	16*h*	1	0	0.4266(14)	0.0484(4)	0.018(2)
O5	16*h*	1	−0.2436(13)	1/4	−0.0373(4)	0.021(3)
Li	8*e*	1	1/2	1/4	−0.0409(17)	0.022(8)*

Note. The U_{eq} values are defined by $U_{eq} = 1/3(\sum i \sum j U_{ij} a_i^* a_j^* a_i a_j)$.

Table 4
Anisotropic displacement parameters (Å^2) for $Li_2(UO_2)_3(VO_4)_2O$

Atom	U_{11}	U_{22}	U_{33}	U_{12}	U_{13}	U_{23}
U1	0.0098(4)	0.0098(4)	0.0114(5)	0.00000	0.00000	0.00000
U2	0.0122(5)	0.0101(4)	0.0084(4)	0.00000	0.00000	0.00000
V	0.0113(17)	0.0079(15)	0.0108(15)	0.00000	0.00000	0.00000
O1	0.007(6)	0.007(6)	0.025(12)	0.00000	0.00000	0.00000
O2	0.013(5)	0.022(6)	0.026(6)	0.00000	0.003(5)	0.00000
O3	0.003(8)	0.028(10)	0.023(9)	0.00000	0.00000	0.00000
O4	0.031(6)	0.006(5)	0.016(5)	0.00000	0.00000	−0.002(4)
O5	0.004(5)	0.022(6)	0.038(7)	0.00000	0.000(5)	0.00000

Note: The anisotropic displacement factor exponent takes the form $-2\pi^2[h^2a^{*2}U_{11}+k^2b^{*2}U_{22}+l^2c^{*2}U_{33}+\cdots+2kla^*c^*U_{23}]$

range 20–1200 °C with heating and cooling rate 2 °C/mn using platinum crucibles. DTA measurements showed that both compounds incongruently melt at 950 and 980 °C for A = Li and Na, respectively.

3. Crystal structure description and discussion

Table 5 provides selected metal to oxygen distances, uranyl angles and bond valences calculated using Brese and O'Keeffe data [17] with $b = 0.37$ Å except for U–O bonds for which the coordination independent parameters ($R_{ij} = 2.051$ Å, $b = 0.519$ Å) were taken from Burns et al. [18].

In $Li_2(UO_2)_3(VO_4)_2O$, there are two symmetrically independent uranium atoms U(1) and U(2) in 4*b* and 8*e* special sites, respectively; U(1) with a square bipyramid coordination of oxygen atoms and U(2) surrounded by seven oxygen atoms in a pentagonal bipyramidal environment. In both cases, two oxygen atoms at short distances create a uranyl ion $UO2^{2+}$. In the U(1)O6 square bipyramid, the uranyl ion is perfectly linear with two U(1)–O(3) bond lengths of 1.80(2) Å. In the equatorial plane, the four O(2) oxygen atoms at 2.28(1) Å of U(1) form a weakly distorted square, with O(2)–U(1)–O(2) angles of 90.5(1)°. In the $U(1)O_6$ polyhedron, the O(2)–U(1)–O(3) angles are 84.55(25) and 95.45(25). In $U(2)O_7$ pentagonal bipyramids with *mm*2 symmetry, the $U(2)O(5)_2^{2+}$ uranyl ion is not perfectly linear (176.19(4)°) and the U–O(5) distances being equal to 1.79(1) Å, weakly shorter than those of $U(1)O_2^{2+}$ ion. In the equatorial plane, two pairs of oxygen atoms, O(4)–U(2)–O(4), are situated at 2.38(1) and 2.53(1) Å , respectively, the fifth oxygen atom O(1) being significantly nearer at 2.105(1) Å. The increase of the average equatorial U–O bonds from 6 to 7 coordinations is in agreement with the values reported by Burns [19] from the analysis of numerous well-refined structures, 2.264 and 2.368 Å, respectively.

The only independent vanadium atom is situated in 8*f* special site with a tetrahedral environment of oxygen atoms with two O(4) at 1.70(1) and two O(2) at 1.71(1) Å and bond angles of 98.9(5)° and 108.7(5)° for O(4)–V–O(4) and O(2)–V–O(2), respectively.

Table 5
Interatomic distances (Å), valence bonds and uranyl angles (deg.) in $Li_2(UO_2)_3(VO_4)_2O$

U1 environment			*U2 environment*		
	d_{U-O}	s_{ij}		d_{U-O}	s_{ij}
U1—O3 (2 ×)	1.798(15)	1.628	U2—O5 (2 ×)	1.787(9)	1.663
U1—O2 (4 ×)	2.284(11)	0.638	U2—O1	2.105(1)	0.901
$\sum s_{ij}$		5.808	U2—O4 (2 ×)	2.380(11)	0.530
			U2—O4 (2 ×)	2.526(10)	0.400
			$\sum s_{ij}$		6.087
V environment			*Li environment*		
	d_{V-O}	s_{ij}		d_{V-O}	s_{ij}
V–O4 (2 ×)	1.704(11)	1.307	Li–O5 (2 ×)	1.881(9)	0.305
V–O2 (2 ×)	1.712(12)	1.279	Li–O3	2.290(4)	0.102
$\sum s_{ij}$		5.172	Li–O2 (2 ×)	2.320(35)	0.094
			$\sum s_{ij}$	0.900	
O3—U1—O3	180		O5–U2–O5	176.3(7)	

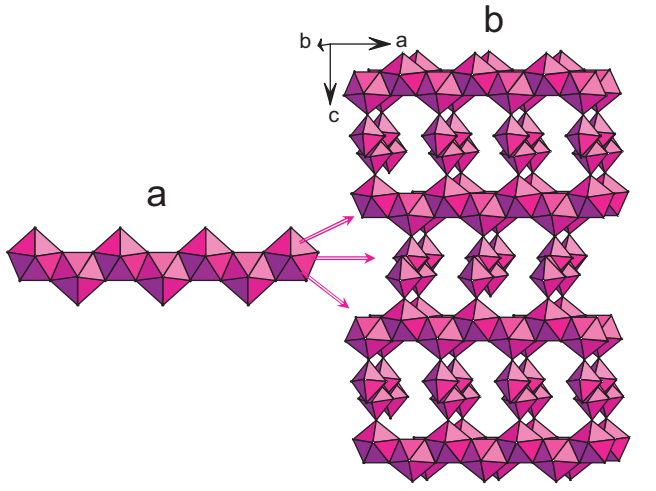

Fig. 1. The $^1_\infty[UO_5]^{4-}$ uranyl infinite chain (a), and the 3-D framework of perpendicular $^1_\infty[UO_5]^{4-}$ chains in $Li_2[(UO_2)_3(VO_4)O]$ (b).

The $U(2)O_7$ pentagonal bipyramids share opposite edges O(4)–O(4) to form infinite zig-zag chains $^1_\infty[UO_5]^{4-}$, Fig. 1a. The $^1_\infty[UO_5]^{4-}$ chain of edge-sharing UO_7 pentagonal bipyramids is the most familiar arrangement found in uranyl compounds. In most structures, the chains are parallel to each other and can be connected in many ways to form planar or corrugated sheets. In $Li_2(UO_2)_3(VO_4)_2O$ they are perpendicular to each other and extend along the $\vec{b}$-axis at $z\sim0$ and $z\sim\frac{1}{2}$ and down the $\vec{a}$-axis at $z\sim\frac{1}{4}$ and $z\sim\frac{3}{4}$. To our knowledge, the only example of mineral compound containing $^1_\infty[UO_5]^{4-}$ chains running in two perpendicular directions is that of soddyite, $(UO_2)_2SiO4\cdot2H_2O$ [20], where uranyl chains are connected through SiO_4 tetrahedra. Recently, monovalent cation uranyl vanadates $A(UO_2)_4(VO_4)_3$ (A = Li, Na) (8) provided another interesting example. The recently described compound $[(UO_2)_3(PO_4)O(OH)(H_2O)_2](H_2O)$ contains also non-intersecting chains connected through PO_4 tetrahedra but the chains are built from dimmers of edge shared UO_7

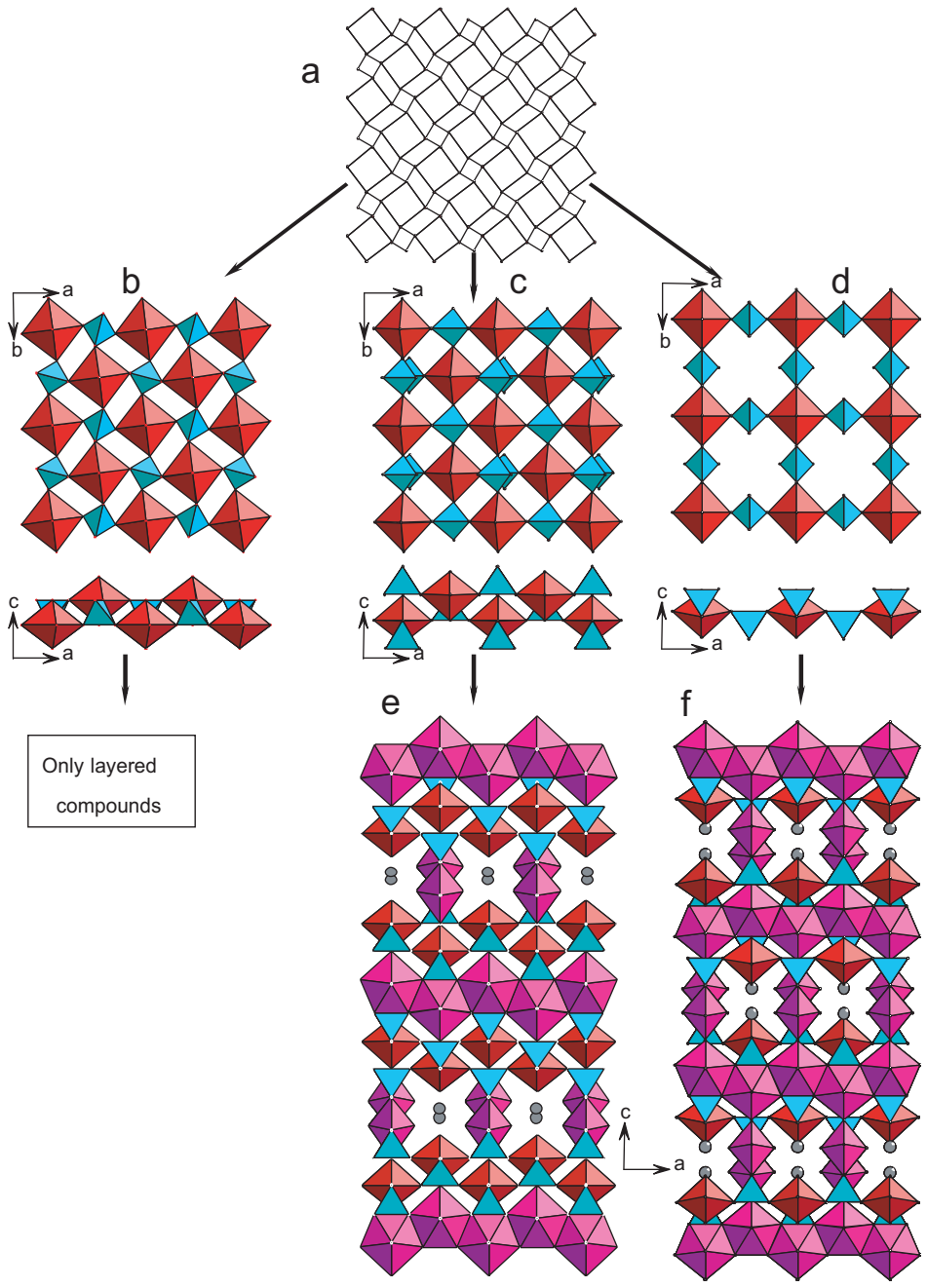

Fig. 2. The autinite anion topology (a), the autinite—type sheet obtained in uranyl phosphates and uranyl arsenates (b), the $^{2}_{\infty}[(UO_2)_2(VO_4)_3]^{5-}$ sheet in the $A(UO_2)_4(VO_4)_3$ (A = Li, Na) compounds, (c), the $^{2}_{\infty}[(UO_2)(VO_4)_2]^{4-}$ sheet in the $A_2(UO_2)_3(VO_4)_2O$ (A = Li, Na) compounds where half of the UO_6 square bipyramids are removed (d). The $^{1}_{\infty}[UO_5]^{4-}$ chains are hung on the two types of sheets to built the 3-D arrangements of $A(UO_2)_4(VO_4)_3$ (e) and $A_2(UO_2)_3(VO_4)_2O$ (f) compounds.

pentagonal bipyramids further linked by UO_8 hexagonal bipyramids [21]. In $Li_2(UO_2)_3(VO_4)_2O$, the $^{1}_{\infty}[UO_5]^{4-}$ chains are connected together by sharing the equatorial oxygen atoms O(1) creating a 3-D arrangement of UO_7 pentagonal bipyramids, Fig. 1b. The UO_6 square bipyramids are linked to this framework through VO_4 tetrahedra. In fact, the UO_6 square bipyramids and VO_4 tetrahedra form $^{2}_{\infty}[(UO_2)(VO_4)2]^{2-}$ sheets, Fig. 2d, parallel to the (0 0 1) plane of the tetragonal cell, with autinite anion topology [19,22], Fig. 2a. In these sheets, squares population is similar to that found in $K_4[(UO_2)(PO_4)_2]$ [23], with one eighth of the squares occupied by the UO6 square bipyramids and one quarter by the VO_4 tetrahedra. The non-shared edges of the VO_4 tetrahedra are located up and down relative to the plane of the layer and are parallel to the $\vec{a}$ and $\vec{b}$ axes, respectively. This allows attachment to these edges of the $^{1}_{\infty}[UO5]^{4-}$ chains. Note that the equatorial oxygen atoms shared between two perpendicu-

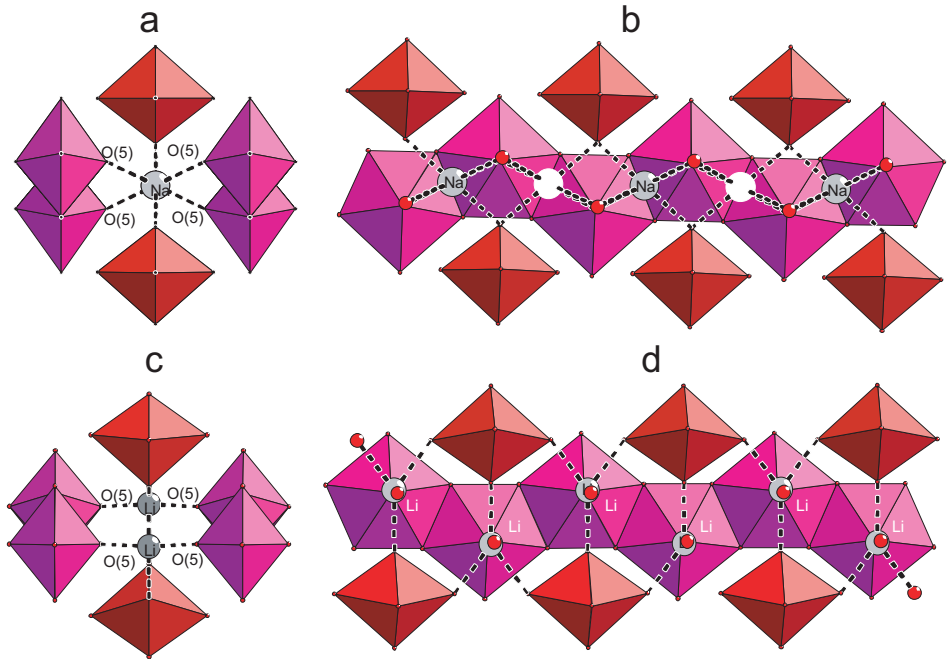

Fig. 3. The channels created by the 3-D arrangement are formed by face—shared octahedra. The octahedra are occupied by Na^+ ions (a, b). The Li^+ ions are displaced at the middle of oxygen O(5)–O(5) edge (c, d).

lar $^1_\infty[UO5]^{4-}$ chains on each side of the layer occupy the centers of the squares of the autunite anion topology non-occupied by UO_6 square bipyramids.

It is noticeable that while autunite-type sheets are the most common sheets for layered uranyl phosphates and uranyl arseniates [24–35], they are never found in layered uranyl vanadates for which sheets based on Francevillite anion topology are preferred and contain vanadium in square pyramidal coordination [1,2,36–40]. On the opposite, for the two series $A(UO_2)_4(VO_4)_3$ (8) and $A_2(UO_2)_3(VO_4)_2O$ (A = Li, Na), the 3-D frameworks contain uranyl-vanadate sheets derived from the autinite anion topology. The autinite-type sheet (Fig. 2b) itself cannot be used as a basis for construction of such 3-D frameworks, indeed all the vertices of the PO_4 tetrahedra are shared with UO_6 square bipyramids, moreover, the PO_4 tetrahedra are "protected" by two layers of UO_6 polyhedra; in $A(UO_2)_4(VO_4)_3$ [8] a tetrahedron on two is removed and replaced by two tetrahedra attached above and below the layer (Fig. 2c); in the present compounds $A_2(UO_2)_3(VO_4)_2O$, half the square bipyramids are removed and half tetrahedra undergo a rotation of 180°, Fig. 2d. Thus, in both compounds above the sheet, all the non-shared O–O edges are parallel to [010], whereas all edges below the sheet are parallel to [100] and are all accessible to $^1_\infty[UO_5]^{4-}$ chains to form 3-D frameworks, Fig. 2e and f.

The 3-D frameworks create similar nearly circular channels running alternately along [010] and [100] and limited by uranyl oxygen ions only (Fig. 2e and f). The channels are built of face-shared O_6 distorted octahedra. In $Na(UO_2)_4(VO_4)_3$, the Na^+ ions occupy half of the octahedra (Fig. 3a) and are above the middle of the edge shared between two $(UO_2)O_5$ polyhedra of a $^1_\infty[UO_5]^{4-}$ chain (Fig. 3b). In $Li_2(UO_2)_3(VO_4)_2O$, the octahedral sites are empty; the Li^+ ions occupy entirely the particular 8*e* sites at the middle of the O(5)–O(5) edges of the shared octahedral face, (Fig. 3c), leading to two short Li–O(5) distances of 1.881(9) Å. The Li atoms are above the center of the $(UO_2)O_5$ polyhedra, Fig. 3d. The Li environment is completed in the equatorial plane three oxygen atoms at larger distances, one O(3) at 2.29(4) Å and two O(2) at 2.32 (4) Å leading to a distorted trigonal bipyramid around Li.

On the basis of U–O, V–O and Li–O distances, the calculated bond valence sums are 5.81 v.u. for U(1), 6.09 v.u. for U(2), 5.17 v.u. for V, and 0.90 v.u. for Li. These values are consistent with formal valences of U^{6+}, V^{5+} and Li^+. The bond valence sums for the O atoms are in the range from 1.73 to 2.01 v.u.

If we assume that Li occupy the same positions within the channels in $Li(UO_2)_4(VO_4)_3$, the position and the strong Li–O(5) bonds explain the decrease of the conductivity and the increase of the activation energy observed from Na to Li in the $A(UO_2)_4(VO_4)_3$ (A = Li, Na) compounds [8]. Ionic conductivity measurements were carried out for $Li_2(UO_2)_3(VO_4)_2O$ and the temperature dependence of the conductivity is compared with that of $Li(UO_2)_4(VO_4)_3$ in Fig. 4. The observed linear evolution of $\log\sigma$ with temperature reverse shows that the ionic conductivity obeys to the Arrhenius law over the studied temperature range, with activation energy values of 0.76 eV. The observed conductivity is significantly weaker than that of $Li(UO_2)_4(VO_4)_3$ with a larger activation energy due to the full occupancy of the O(5)–O(5) edges.

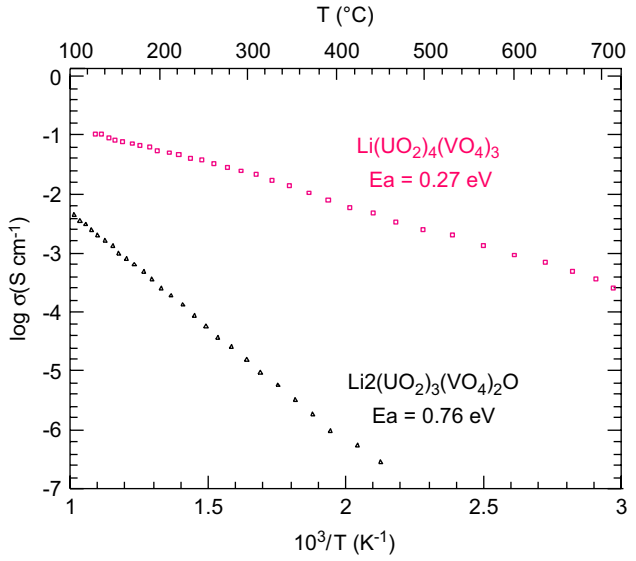

Fig. 4. Arrhenius plots and comparison of electrical conductivity of $Li_2(UO_2)_3(VO_4)_2O$ and $Li(UO_2)_4(VO_4)_3$ compounds.

4. Conclusion

Whereas sheets with autunite-type anion topology do not exist in the layered uranyl vanadates, the $A_2(UO_2)_3(VO_4)_2O$ (A = Li, Na) compounds constitute after the $A(UO_2)_4(VO_4)_3$ (A = Li, Na) series (8), the second example of 3-D arrangement of parallel sheets derived from the autunite-type anion topology connected by alternately perpendicular chains of edge-shared $(UO_2)O_5$ pentagonal bipyramids. In the two series, similar non-intersecting perpendicular tunnels are created. The variation of the conductivity properties of these compounds is related to the different occupations (position and occupancy rate) of the tunnels by the alkali metal. It would be interesting to verify that Li and Na occupy the same sites in the two series, so we continue our attempts for obtaining single crystals of $Li(UO_2)_4(VO_4)_3$ and $Na_2(UO_2)_3(VO_4)_2O$.

References

[1] F. Abraham, C. Dion, M. Saadi, J. Mater. Chem. 3 (1993) 459.
[2] F. Abraham, C. Dion, N. Tancret, M. Saadi, Adv. Mater. Res. (1994) 511.
[3] I. Duribreux, M. Saadi, S. Obbade, C. Dion, F. Abraham, J. Solid State Chem. 172 (2003) 351.
[4] C. Dion, S. Obbade, E. Rackelboom, M. Saadi, F. Abraham, J. Solid. State Chem. 155 (2000) 342.
[5] S. Obbade, C. Dion, L. Duvieubourg, M. Saadi, F. Abraham, J. Solid State Chem. 173 (2003) 1.
[6] S. Obbade, C. Dion, M. Saadi, F. Abraham, J. Solid State Chem. 177 (2004) 1567.
[7] I. Duribreux, F. Abraham, C. Dion, M. Saadi, J. Solid State Chem. 146 (1999) 258.
[8] S. Obbade, C. Dion, M. Rivenet, M. Saadi, F. Abraham, J. Solid State Chem. 177 (2004) 2058.
[9] D.E. Appleman, H.T. Evans, Am. Miner. 50 (1965) 825.
[10] P.G. Dickens, G.P. Stuttard, R.G.J. Ball, A.V. Powell, S. Hull, S. Patat, J. Mater. Chem. 2 (1992) 161.
[11] G. Smith, R.J. Snyder, J. Appl. Crystallogr. 12 (1979) 60.
[12] SAINT Plus Version 5.00, Bruker Analytical X-ray Systems, Madison, W1, 1998.
[13] SHELXTL NT, Program Suite for Solution and Refinement of Crystal Structure Version 5.1, Bruker Analytical X-rays Systems Madison W1, 1998.
[14] R.H. Blessing, Acta Crystallogr. A51 (1995) 33.
[15] G.M. Sheldrick, SHELXS-86, Program for Crystal Structure Determination, University of Göttingen, Germany, 1986.
[16] J.A. Ibers, W.C. Hamilton (Eds.), International Tables for X-ray Crystallography, vol. IV, Kynoch Press, Birmingham, UK, 1974.
[17] N.E. Bresse, M. O'Keeffe, Acta Crystallogr. B47 (1991) 192.
[18] P.C. Burns, R.C. Ewing, F.C. Hawthorne, Can. Miner. 35 (1997) 1551.
[19] P.C. Burns, Can. Miner. 43 (2005) 1839.
[20] F. Demartin, C.M. Gramaccioli, T. Pilati, Acta Crystallogr. B48 (1992) 1.
[21] P.C. Burns, C.M. Alexopoulos, P.J. Hotchkiss, A.J. Locock, Inorg. Chem. 43 (6) (2004) 1816.
[22] P.C. Burns, M.L. Miller, R.C. Ewing, Can. Miner. 34 (1996) 845.
[23] S.A. Linde, Y.E. Gorbunova, A.V. Lavrov, Zh. Neorg. Khim. 25 (1980) 1992.
[24] I.L. Botto, E.J. Baran, P.J. Aymonino, Z. Chem. 16 (1975) 163.
[25] B. Morosin, Acta Crystallogr. B34 (1978) 3732.
[26] B. Morosin, Phys. Lett. A65 (1978) 53.
[27] A.N. Fitch, A.F. Wright, B.E.F. Fender, Acta Crystallogr. B38 (1982) 1108.
[28] A.N. Fitch, B.E.F. Fender, Acta Crystallogr. C 39 (2) (1983) 162.
[29] A.N. Fitch, L. Bernard, A.T. Howe, A.F. Wright, B.E.F. Fender, Acta Crystallogr. C 39 (2) (1983) 159.
[30] A.N. Fitch, M. Cole, Mater. Res. Bull. 26 (5) (1991) 407.
[31] A.J. Locock, P.C. Burns, M.J.M. Duke, T.M. Flynn, Can. Miner. 42 (4) (2004) 973.
[32] A.J. Locock, P.C. Burns, T.M. Flynn, Can. Miner. 42 (6) (2004) 1699.
[33] A.J. Locock, P.C. Burns, J. Solid State Chem. 177 (8) (2004) 2675.
[34] A.J. Locock, P.C. Burns, T.M. Flynn, Can. Miner. 43 (2) (2005) 721.
[35] A.J. Locock, P.C. Burns, T.M. Flynn, Can. Miner. 43 (2) (2005) 847.
[36] F. Cesbron, N. Morin, Bul. Soc. Fr. Miner. Cristallogr. 91 (5) (1968) 453.
[37] D.P. Shashkin, Doklady Akad. Nauk SSSR 220 (6) (1975) 1410.
[38] P. Piret, J.P. Declerco, D. Wauters-Stoop, Bull. Miner. 103 (2) (1980) 17.
[39] K. Mereiter, Neues Jahrbuch fuer Mineralogie, Monatshefte 12 (1986) 552.
[40] K.A. Hughes, P.C. Burns, U. Kolitsch, Can. Miner. 41 (3) (2003) 677.